A Pulse EPR and ENDOR Investigation of the Electronic and Geometric Structure of Cobaltous Tetraphenylporphyrin(Pyridine)

Sabine Van Doorslaer, Rainer Bachmann, and Arthur Schweiger*

Physical Chemistry Laboratory, Swiss Federal Institute of Technology, 8092 Zürich, Switzerland

Received: January 19, 1999; In Final Form: March 23, 1999

Different pulse Electron Paramagnetic Resonance (EPR) and Electron Nuclear DOuble Resonance (ENDOR) techniques are used to study the electronic and geometric structure of (tetraphenylporphyrinato)cobaltate(II) with pyridine as an axial ligand (cobaltous tetraphenylporphyrin(pyridine), CoTPP(py)). This complex is considered as a model for the heme group in deoxygenated hemoglobin and myoglobin. For the first time, the small hyperfine and nuclear quadrupole interactions of the porphyrin nitrogens of CoTPP(py) are determined using three-pulse electron spin−echo envelope modulation (ESEEM), hyperfine sublevel correlation (HYSCORE), and double nuclear coherence transfer (DONUT)−HYSCORE spectroscopy as well as Davies-ENDOR, and hyperfine correlated ENDOR (HYEND). The assignment of the different cross-peaks in the HYSCORE spectra is shown to be considerably facilitated by the DONUT−HYSCORE experiment. Furthermore, the hyperfine interactions of the surrounding protons are investigated by Davies- and Mims-ENDOR and HYSCORE spectroscopy at X- and S-band microwave frequencies. For the first time, the potential of proton HYSCORE spectroscopy at S-band is demonstrated. Assignment of the observed couplings is facilitated using deuterated pyridine as the axial ligand. The interactions with the ortho and meta protons of pyridine and with the protons of the porphyrin ligand are determined. From the Davies-ENDOR spectra of CoTPP(py) and CoTPP([^{15}N]py), the hyperfine and nuclear quadrupole couplings of the pyridine nitrogen are evaluated. From the hyperfine and nuclear quadrupole parameters, structural (internuclear distances) and electronic information is derived. Comparisons are made with known EPR and ENDOR studies on a number of porphyrin systems with different metal ions. The similarities and differences are discussed in detail.

Introduction

Hemoglobin (Hb) and myoglobin (Mb) are iron-containing heme proteins responsible for the dioxygen storage and transport in biological systems. Because of their enormous biological importance, these heme proteins have been the subject of many spectroscopic studies to determine the structural factors that govern their oxygen affinity. However, the analysis of the electronic and geometric structure is very difficult due to the fast autoxidation rates of these proteins and the fact that they are diamagnetic and therefore EPR silent.

In the presence of a single nitrogen base, Co(II) porphyrin complexes show the ability for reversible addition of molecular oxygen.[1] Both the oxygenated and the deoxygenated Co(II) adducts are paramagnetic and can thus be studied by EPR. The autoxidation rate of the oxy Co(II) complexes is slower than in the case of the ferrous native proteins. Due to these unique features, Co(II) porphyrin complexes have become of special interest as model systems for Hb and Mb. (For a survey, see refs 2 and 3.) Furthermore, the chemical substitution of ferrous protoporphyrin IX with cobaltous porphyrin in Hb and Mb[4] opened the way to study both the oxy and deoxy species of the proteins with continuous wave (CW) EPR and ENDOR techniques.[5−7]

For several decades, synthetic cobalt porphyrin systems have been the subject of numerous spectroscopic investigations, including EPR and ENDOR studies.[2,3] The majority of the studies on pentacoordinated Co(II) porphyrin complexes and their corresponding oxygenated forms were done using CW EPR.[1,2,8−11] Some of these complexes were also investigated using CW ENDOR.[12−14] Within the last 2 decades, a variety of one- and two-dimensional pulse EPR[15] and pulse ENDOR[16] schemes have been introduced that allow one to characterize a paramagnetic compound in much greater detail than with the classical CW EPR and CW ENDOR experiments. Apart from some three-pulse electron spin−echo envelope modulation (ESEEM) studies on oxygenated Co(II) porphyrin complexes,[17−18] these techniques have not been used to investigate synthetic cobalt containing porphyrin systems.

In this paper, we report on pulse EPR and ENDOR studies of a frozen solution of (tetraphenylporphyrinato)cobaltate(II) to which there is an axially coordinated pyridine ligand (cobaltous tetraphenylporphyrin(pyridine), CoTPP(py)) (Figure 1). This complex has already been investigated using CW EPR[2,9] and CW ENDOR.[14] However, the use of pulse EPR and ENDOR techniques at two microwave (mw) frequencies (S-band (2−4 GHz) and X-band (8−10 GHz)) enables us to study this complex in far greater detail. For the first time, the hyperfine and quadrupole couplings of the porphyrin nitrogens of CoTPP(py) have been evaluated. Furthermore, the hyperfine interactions of the surrounding protons have been determined. Däges et al.[14] already mentioned the observation of proton couplings in the CW ENDOR spectra of CoTPP(py), but they did not determine the hyperfine parameters. The hyperfine and nuclear quadrupole couplings of the pyridine nitrogen obtained from our analysis turn out to differ from those reported earlier. Finally, the observed interactions are interpreted in terms of internuclear distances and spin distributions. Comparisons are made with known data for different metalloporphyrin complexes.

10.1021/jp9902248 CCC: $18.00
Published on Web 07/15/1999

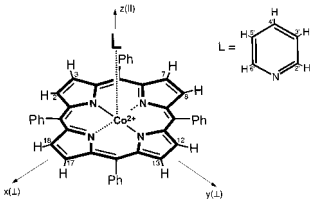

Figure 1. Structure of cobaltous tetraphenylporphyrin(pyridine) and definition of the *x*-, *y*-, and *z*-axes.

Materials and Methods

Sample Preparation. Tetraphenylporphyrinato)cobaltate(II), CoTPP, was bought from Aldrich and was used without further purification. Pyridine was purchased from Fluka (pro analysis). As a solvent absolute toluene (Fluka, puriss., absolute, over molecular sieves) was used. Deuterated pyridine (py-d_5) (>99% purity) was purchased from CIBA and ^{15}N-labeled pyridine ([^{15}N]py) (>98% purity) was obtained from Cambridge isotope Laboratories. The porphyrin complex was dissolved in toluene containing about 10 mM of pyridine. The final concentration of the CoTPP(py) complex was about 1 mM. After the components were mixed, the solution was transferred to an EPR tube. Oxygen-free samples were obtained by degassing on a vacuum line using the usual freeze−pump−thaw method.

^{15}N-labeled (> 99% purity) cobaltic tetraphenylporphyrin chloride, Co(III)[^{15}N]TPPCl was bought from Porphyrin Products, Inc. To reduce Co(III)[^{15}N]TPPCl to the cobaltous state, it was dissolved in degassed CH_2Cl_2 in a concentration of 14 mM and then mixed with an equal volume of a solution of $Na_2S_2O_4$ in degassed H_2O (57 mM) for about 1 h. The CH_2Cl_2 phase was separated from the aqueous phase and vacuum distilled. The remaining Co(II)[^{15}N]TPP was then treated in the same way as described above.

Equipment. CW EPR measurements are performed on both a Bruker ESP300 spectrometer (mw frequency 9.48 GHz) equipped with a liquid nitrogen cryostat and a Bruker ESP380 spectrometer (microwave frequency 9.71 GHz) with cooling equipment from Oxford and Cryogenics. The frozen solution spectrum is measured at 85 K with a mw power of 2 mW, a modulation amplitude of 0.05 mT, and a modulation frequency of 100 kHz.

The pulse EPR and ENDOR experiments are carried out on a pulse X-band Bruker ESP380 spectrometer and on a home-built pulse S-band EPR spectrometer (microwave frequency 2−4 GHz).[19] All the measurements are done in frozen solutions at a temperature of 15 K and a repetition rate of 1 kHz.

The Following Pulse Sequences Were Used. *Three-pulse ESEEM:*[15,20] *Pulse Sequence* $\pi/2-\tau-\pi/2-T-\pi/2-\tau-$*Echo.* At X-band, pulse lengths $t_{\pi/2} = 8$ ns, a starting time $T_0 = 96$ ns, and a time increment $\Delta T = 16$ ns (512 time intervals) are used. To get rid of the blind spot behavior, time τ is varied in steps of $\Delta\tau = 8$ ns, with a starting value $\tau_0 = 96$ ns (128 time intervals). At S-band, $t_{\pi/2} = 20$ ns, $T_0 = 330$ ns, and $\Delta T = 20$ ns (200 intervals) are used and τ is varied in steps of $\Delta\tau = 10$ ns (20 intervals). A four-step phase cycle is used in all experiments.

HYSCORE:[21−23] *Pulse Sequence* $\pi/2-\tau-\pi/2-t_1-\pi-t_2-\pi/2-\tau-$*Echo*. At X-band, $t_{\pi/2} = 24$ ns, $t_\pi = 16$ ns, starting times $t_{01} = 96$ ns, and $t_{02} = 96$ ns and time increments $\Delta t_1 = 16$ ns, $\Delta t_2 = 16$ ns (data matrix 512 × 512) for 6 τ values (96, 176, 232, 296, 344, and 424 ns), and an eight-step phase cycle are used. At S-band, $t_{\pi/2} = 20$ ns, $t_\pi = 12$ ns, $t_{01} = 420$ ns, $t_{02} = 420$ ns, $\Delta t_1 = 20$ ns and $\Delta t_2 = 20$ ns (data matrix 150 × 150) for 3 τ values (330, 505, and 765 ns), and a four-step phase cycle are used.

DONUT-HYSCORE[24,25] *(X-band).* The pulse sequence $\pi/2-\tau_1-\pi/2-t_1-\pi-\tau_2-\pi-t_2-\pi/2-\tau_1-$echo, with $t_{\pi/2} = 24$ ns, $t_\pi = 16$ ns, $\tau_1 = 96$ ns, $\tau_2 = 344$ ns, $t_{01} = 96$ ns, $t_{02} = 96$ ns, $\Delta t_1 = 16$ ns, $\Delta t_2 = 16$ ns (data matrix 450 × 450), and an eight-step phase cycle are used. τ_1 and τ_2 are chosen so as to minimize the blind spot dependence in the frequency area of interest.

Mims-ENDOR[26] *(X-band).* The pulse sequence $\pi/2-\tau-\pi/2-T-\pi/2-\tau-$echo, with a selective radio frequency (rf) π-pulse of variable frequency ν_{rf} applied during time T, and $t_{\pi/2} = 16$ ns, $t_\pi^{rf} = 10$ (8.5) μs, $T = 12$ (10.5) μs, $\tau_0 = 88$ ns, $\Delta\tau = 8$ ns (128 or 256 time intervals in order to remove the blind spots) are used. An rf increment of 50 kHz is used.

Davies-ENDOR[27] *(X-band).* The pulse sequence $\pi(1)-T-\pi/2-\tau-\pi(2)-\tau-$echo, with a selective rf π-pulse of variable frequency ν_{rf} applied during time T, $t_\pi(1) = 96$ ns, $t_{\pi/2} = 48$ ns, $t_\pi(2) = 96$ ns, $t_\pi^{rf} = 10$ (8.5) μs, $\tau = 104$ ns, and $T = 12$ (10.5) μs is used. An rf increment of 50 kHz is used.

HYEND[28] *(X-band).* The pulse sequence $\pi(1)-t-\pi(2)-T-\pi(2)-t-\pi/2-\tau-\pi(3)-\tau-$echo, with two selective rf $\pi/2$-pulses of variable frequency ν_{rf} applied during the time intervals t, and $t_\pi(1) = 96$ ns, $t_{\pi/2}^{rf} = 4.25$ μs, $t_\pi(2) = 96$ ns, $T_0 = 304$ ns, $t_{\pi/2} = 48$ ns, $\tau = 104$ ns, and $t_\pi(3) = 96$ ns is used. The time T is incremented in steps of 8 ns (1024 points). The rf increment is taken 50 kHz.

Data Manipulation. Data processing is done with MATLAB 5.1. (The MathWorks, Inc.). The ESEEM time-domain data are baseline corrected with a third-order polynomial, apodized with a Hamming window and zero filled. In addition, the HYSCORE and DONUT-HYSCORE spectra are apodized using a Hanning window along the diagonal. After 1D or 2D Fourier transformation, the absolute-value spectra are calculated. To get rid of blind spots and deadtime dependent distortions in the Mims-ENDOR, three-pulse ESEEM, HYSCORE, and DONUT−HYSCORE experiments, the spectra are measured at different τ values and added together.

Theory. The spin Hamiltonian for a paramagnetic species with a Co^{2+} ion (electron configuration $3d^7$, $S = {}^1/_2$, $I = {}^7/_2$) and ^{14}N nuclei and protons is given by

$$H = \frac{\beta_e}{h}\mathbf{B}_0\mathbf{g}\mathbf{S} + \mathbf{S}\mathbf{A}^{Co}I + H_{nucl} \qquad (1)$$

The first term is the electron Zeeman interaction, the second term describes the hyperfine interaction between the unpaired electron, and the nuclear spin of cobalt. The CW EPR spectrum of a frozen solution of CoTPP(py) is mainly dominated by these two terms.

H_{nucl} describes the interactions with the surrounding nitrogen nuclei and protons, which can be observed with ESEEM and ENDOR. For these experiments, the observer positions have to be carefully chosen in order to scan through all the molecular orientations contributing to the CW EPR spectrum (orientation selection[29]). The analysis of the ESEEM spectra is based on the following equations.

(a) $S = {}^1/_2$, $I = {}^1/_2$ *Systems (Interactions with* ^{1}*H and* ^{15}*N).* The nuclear transition frequencies in the two m_S manifolds are given by

$$\nu_{\alpha(\beta)} = \left[\left(\frac{A}{2} \pm \nu_I\right)^2 + (B/2)^2\right]^{1/2} \qquad (2)$$

with the nuclear Zeeman frequency $\nu_I = -g_n\beta_n B_0/h$. For an axially symmetric **g** and hyperfine **A** matrix, $g_\parallel$ chosen along the *z*-axis and a nucleus lying in the *xz*-plane, A and B are defined by[30−33]

$$A = a_{iso} + T[(3/g^2)(g_{||}^2 \cos\theta \cos\beta + g_{||}^2 \sin\theta \sin\beta \cos\phi) \times (\cos\theta \cos\beta + \sin\theta \sin\beta \cos\phi) - 1] \quad (3)$$

and

$$B^2 = B'^2 + C'^2$$

with

$$B' = T\left[(3/g^2)(g_{||}^2 \cos\theta \cos\beta + g_{\perp}^2 \sin\theta \sin\beta \cos\phi) \times (\cos\theta \sin\beta \cos\phi - \sin\theta \cos\beta) + (a_{iso}/T - 1) \times \frac{(g_{\perp}^2 - g_{||}^2)}{g^2} \sin\theta \cos\theta\right] \quad (4)$$

$$C' = T(3/g^2)(g_{||}^2 \cos\theta \cos\beta + g_{\perp}^2 \sin^2\theta \sin\beta \cos\phi) \sin\beta \sin\phi \quad (5)$$

and

$$g^2 = g_{||}^2 \cos^2\theta + g_{\perp}^2 \sin^2\theta \quad (6)$$

Here β is the angle between the vector **r**, joining the electron spin and the nucleus, and the $g_{||}$ principal axis. The polar angles θ and ϕ define the orientation of the magnetic field vector in the *x*,*y*,*z*-frame,[30] a_{iso} denotes the isotropic hyperfine constant, and

$$T = \left(\frac{\mu_0}{4\pi}\right)\frac{g g_n \beta_e \beta_n}{r^3 h} \quad (7)$$

is the point−dipole interaction. Note that in these formulas the hyperfine interaction is assumed to consist only of a point−dipolar and an isotropic contribution.

From the values of a_{iso} and *r*, the hyperfine matrix elements can be calculated by[32]

$$A_{ij} = a_{iso} + \frac{\mu_0}{4\pi}\frac{g_n \beta_e \beta_n}{r^3 h} g_i (3 r_i r_j - \delta_{ij}) \qquad (i, j = x, y, z) \quad (8)$$

with $r_x = \sin\beta$, $r_y = 0$; $r_z = \cos\beta$, $g_x = g_y = g_{\perp}$, and $g_z = g_{||}$.

Diagonalization of this matrix leads to the principal values $A_{x'}$, $A_{y'}$, and $A_{z'}$ of the hyperfine matrix.

The HYSCORE (hyperfine sublevel correlation spectroscopy) method[21−23] is a two-dimensional experiment, in which a mixing π-pulse correlates the nuclear coherences of two *different* electron spin (m_S) manifolds. The correlations between the nuclear transitions lead to cross peaks (ν_α,ν_β) and (ν_β,ν_α) in the 2D plots. In the HYSCORE spectra of disordered systems, ridges instead of cross peaks are observed. We made use of the relation

$$B = [8\Delta\nu^S \nu_I/\sqrt{2}]^{1/2} \quad (9)$$

between the maximum displacement $\Delta\nu^S$ of the ridges from the (ν_I,ν_I) diagonal peak and the value of *B* derived by Pöppl et al.[30] *B* is related to *T* and a_{iso} as shown in eqs 4 and 5.

(b) $S = {}^1/_2$, $I = 1$ Systems (Interaction with ^{14}N). The spin Hamiltonian of an $S = {}^1/_2$, $I = 1$ system can be described in terms of the **g** matrix, the hyperfine matrix **A**, and the nuclear quadrupole tensor **Q**. The **Q** tensor is traceless and the principal values Q_x, Q_y, and Q_z are usually expressed by the quadrupole coupling constant $K = e^2qQ/4h$ and the asymmetry parameter η, with $Q_x = -K(1 - \eta)$, $Q_y = -K(1 + \eta)$, and $Q_z = 2K$.

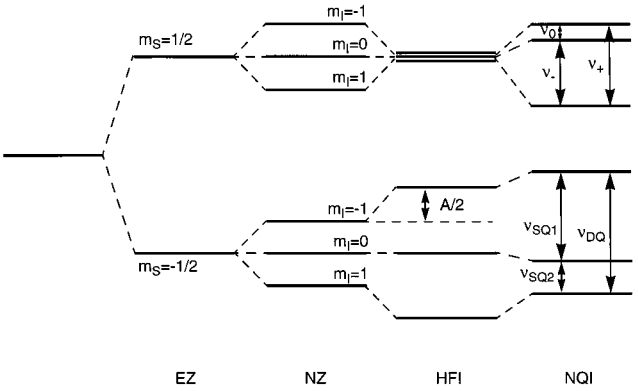

Figure 2. The energy level diagram of an $S = {}^1/_2$, $I = 1$ spin system under the condition of exact cancellation ($\nu_I = |A/2|$). Legends: EZ = electron Zeeman interaction, HFI = hyperfine interaction, NZ = nuclear Zeeman interaction, NQI = nuclear quadrupole interaction, SQ = single quantum, and DQ = double quantum.

In the case of exact cancellation ($|A| \approx 2\nu_I$), the effective field experienced by the nucleus in one of the two m_S manifolds is approximately zero (Figure 2). The ESEEM frequencies within this manifold are therefore close to the true ^{14}N nuclear quadrupole resonance (NQR) frequencies[34]

$$\nu_0 = 2K\eta, \quad \nu_- = K(3 - \eta), \quad \nu_+ = K(3 + \eta) \quad (10)$$

In a HYSCORE experiment, cross peaks are observed between the three frequencies of the upper and the lower m_S manifold. Typical manifestations of HYSCORE spectra of disordered $S = {}^1/_2$, $I = 1$ systems have recently been described by Dikanov et al.[35] In a DONUT−HYSCORE experiment[24−25], nuclear frequencies within the same m_S manifold are correlated with each other. For an $S = {}^1/_2$, $I = 1$ system in exact cancelation, this allows one to observe cross peaks between the NQR frequencies. This additional information may considerably facilitate the identification of the peaks in the HYSCORE spectrum.

Simulation Procedures. The **g** and $\mathbf{A^{Co}}$ principal values obtained from the experimental CW EPR spectrum at 85 K are refined using the program MAGRES.[36] Simulations of the HYSCORE spectra for a disordered $S = {}^1/_2$, $I = {}^1/_2$ system are performed with a computer program based on the equations given above[30] and the ones of Ponti et al.[23] Good starting values for the parameters used in the simulations are obtained by the methods of Pöppl et al.[30] and Dikanov et al.[37] The HYSCORE spectra of disordered $S = {}^1/_2$, $I = 1$ systems are simulated using TRYSCORE.[38] Numerical simulations of the HYEND spectra are carried out with the program package GAMMA.[39] For all other simulations, the MAGRES program package[36] is used.

Results

g and $\mathbf{A^{Co}}$ Matrices. At X-band frequencies, the CW EPR spectrum is found to be axial with well resolved cobalt and pyridine nitrogen hyperfine splittings in the parallel direction (perpendicular to the porphyrin plane). The latter coupling will be discussed later. Based on symmetry considerations, the $g_{||}$ direction is taken perpendicular to the porphyrin plane (along the molecular *z*-axis) in accordance with previous studies.[1,14] The other axes of the molecular frame are taken as indicated in Figure 1. From the line width in the perpendicular direction, a maximum value for $A_{\perp}^{Co}$ can be estimated. Table 1 shows the **g**, $\mathbf{A^{Co}}$, and $A_{||}^{N}$ parameters that were obtained by simulating the experimental CW EPR spectrum using MAGRES.[36] The data agree well with the parameters found in the literature for

TABLE 1: Principal Values of g, A^{Co}, and the $A_{||}^{N}$ Value for CoTPP(py) and CoOEP(py) Derived from CW EPR

	$g_\perp$	$g_{||}$	$A_\perp^{Co}$ (MHz)	$A_{||}^{Co}$ (MHz)	$A_{||}^{N}$ (MHz)	ref
CoTPP(py)	2.324 ± 0.002	2.030 ± 0.002	≤40	236.0 ± 6.0	44.0 ± 4.0	this work
	2.320	2.028		235.5	48.3	14
	2.324	2.027	≤39	236.7	42.6	1
CoOEP(py)	2.326	2.026	ca. 25	231	44	12

TABLE 2: Principal Values of the Proton Hyperfine Interactions of CoTPP(py)[a]

H	$A_{x'}$ (MHz)	$A_{y'}$ (MHz	$A_{z'}$ (MHz)	β (deg)	a_{iso} (MHz)	r (nm)
2′,6′	−7.0 (±0.2)	−7.0 (±0.2)	1.7 (±0.2)	41 (±5)	−4.0 (±0.2)	0.31 (±0.01)
3′,5′	0.4 (±0.1)	0.4 (±0.1)	2.1 (±0.1)	24 (±5)	1.0 (±0.1)	0.52 (±0.01)
2,3,7, 8,12,13,17,18	−0.4 (±0.1)	−0.4 (±0.1)	1.3 (±0.1)	90 (±10)	0.1 (±0.1)	0.53 (±0.01)

[a] a_{iso} is the isotropic hyperfine interaction, r is the distance between the proton and the Co^{2+} ion, and β is the angle between $g_{||}$ and the Co···H direction. ρ(Co) was taken to be 0.95. The numbers in the first column of the table correspond to the one in Figure 1. In the text, the hyperfine couplings are numbered 1, 2, and 3 in order of appearance in the table. $A_{z'}$ is pointing approximately in the direction of the Co nucleus (see eq 8).

both CoTPP(py) and cobaltous octaethylporphyrin(pyridine) (CoOEP(py)). The latter complex is very similar to CoTPP-(py). The parameters in Table 1 are also in good agreement with the ones found for cobalt-substituted Mb and Hb[4−7], illustrating that CoTPP(py) can indeed be considered as a model complex for these systems.

No cobalt ENDOR transitions could be detected, either with pulse or CW ENDOR. This can be ascribed to the nuclear quadrupole interaction ($I = {}^7/_2$) and the large anisotropy of the hyperfine coupling, causing a considerable spread of the ENDOR intensity.

Interaction with the Surrounding Protons. The proton interactions are studied with HYSCORE, Davies-ENDOR, Mims−ENDOR, and HYEND at X- and S-band microwave frequencies and different settings of the magnetic field (orientation selection principle[29]).

In the Davies−ENDOR spectra, taken at several field positons, at least three proton interactions can be distinguished besides the narrow matrix peak at the proton Zeeman frequency. Figure 3a shows the spectrum taken at $g = 2.048$, $\nu_H = 14.44$ MHz (observer position I in the inset). In the corresponding spectrum recorded with fully deuterated pyridine (py-d_5) (Figure 3b), the two largest proton couplings (resonance frequencies indicated by the dashed lines) disappear, indicating that these features represent hyperfine interactions with protons of the pyridine ligand.

The value of the largest proton hyperfine coupling can best be derived from HYSCORE and Davies-ENDOR experiments. The HYSCORE spectra with $\mathbf{B_0} \parallel g_{||}$ at S-band and $\mathbf{B_0} \parallel g_\perp$ at X-band are shown in Figures 4a and c. Figures 3 and 5a and b show Davies-ENDOR spectra taken at observer positions I, II, and III, respectively. (See inset Figure 3.)

For the interpretation of the HYSCORE spectra, we used the formalism described in the theoretical part.[30] It turns out that measurements at S-band frequencies are especially well suited in this case, since the displacements of the HYSCORE ridges along the diagonal depend on $1/\nu_I$ (see eq 9) so that the shifts will be considerably larger at S-band than at X-band. 1D combination peak and 2−pulse experiments are also performed, but the sum combination peak of the largest interaction is greatly masked by the large peak at $2\nu_H$. The latter methods are therefore not very suitable to determine the anisotropic part of the interaction. The values for T and a_{iso} are used as starting values for the simulation. To determine the smaller proton hyperfine interactions, Mims-ENDOR spectra (not shown) and Davies-ENDOR spectra are recorded at several field positions and simulated using MAGRES.[36] Davies-ENDOR is in general considered to be more suited than Mims-ENDOR to study large

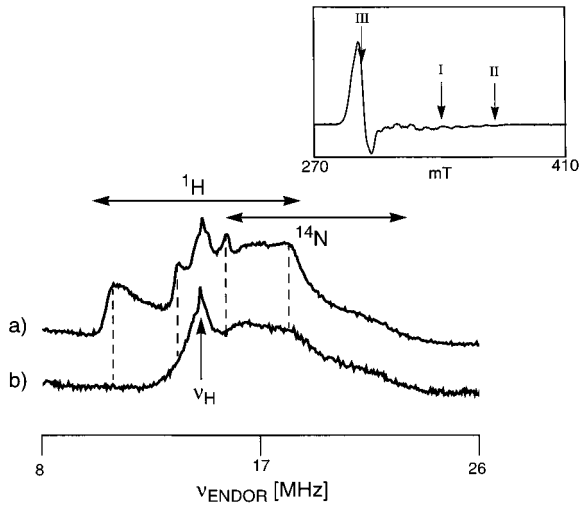

Figure 3. Davies-ENDOR spectra of (a) CoTPP(py) and (b) CoTPP-(py-d_5) at observer position I (see inset: X-band (9.71 GHz) CW EPR spectrum of CoTPP(py) in the 270−410 mT range).

hyperfine couplings.[40] The relative intensity of the proton peak with the largest hyperfine interaction is indeed found to be smaller in the Mims-ENDOR spectra than in the Davies-ENDOR spectra.

The hyperfine parameters found for the three proton interactions are collected in Table 2. These parameters are derived from simulation of the HYSCORE spectra (Figure 4b and d) and the Davies-ENDOR spectra (Figure 5a and b). The corresponding geometric parameters are derived using eq 8 and considering a cobalt spin density ρ(Co) = 0.95.[14] It should be noted that the relative ENDOR intensities of the two m_S manifolds in the simulations are interchanged compared to the experimental Davies-ENDOR spectra. This is not understood, especially since the intensity behavior of the Mims-ENDOR spectra is also opposite to that of the Davies-ENDOR spectra.

Interaction with the Nitrogen Nucleus of the Axial Pyridine Ligand. In the CW EPR spectrum the hyperfine interaction of the ^{14}N nucleus of the pyridine ligand is only resolved along $g_{||}$ (Table 1). To determine all the hyperfine and nuclear quadrupole parameters, Davies-ENDOR spectra of CoTPP([^{14}N]py), CoTPP(py-d_5) and CoTPP([^{15}N]py) are recorded. Due to the large hyperfine couplings (around 40 MHz), ESEEM experiments are not suited in this case. Figure 5a and b show the Davies-ENDOR spectra of CoTPP([^{14}N]py) recorded at the high-field position II ($\mathbf{B}_0 \parallel g_{||}$, $m_I^{Co} = 7/2$) and at $\mathbf{B}_0 \parallel g_\perp$ (observer position III, inset Figure 3), together with the corresponding simulations of the nitrogen spectra. Since the

TABLE 3: Principal Values of the Hyperfine and Nuclear Quadrupole Interaction of the Pyridine Nitrogen in CoTPP(py) and CoOEP(py)

	$A_\perp$ (MHz)	$A_\parallel$ (MHz)	$Q_\perp$ (MHz)	$Q_\parallel$ (MHz)	ref
CoTPP(py)	38.2 (±0.3)	47.4 (±0.1)	0.85 (±0.3)	−1.7 (±0.1)	this work
	38.1	48.6	0.7 (±0.2)	−1.1 (±0.2)	14
CoTPP([^{15}N]py)	−53.3 (±0.2)	−66.3(±0.3)			this work
CoOEP(py)[a]	38.4(±1), 39.15 (±1)	43.4 (±1.0)	1.4 (±0.2), −0.5 (±0.2)	−0.9 (±0.2)	13

[a] Orthorhombic **A** and **Q** are assumed.

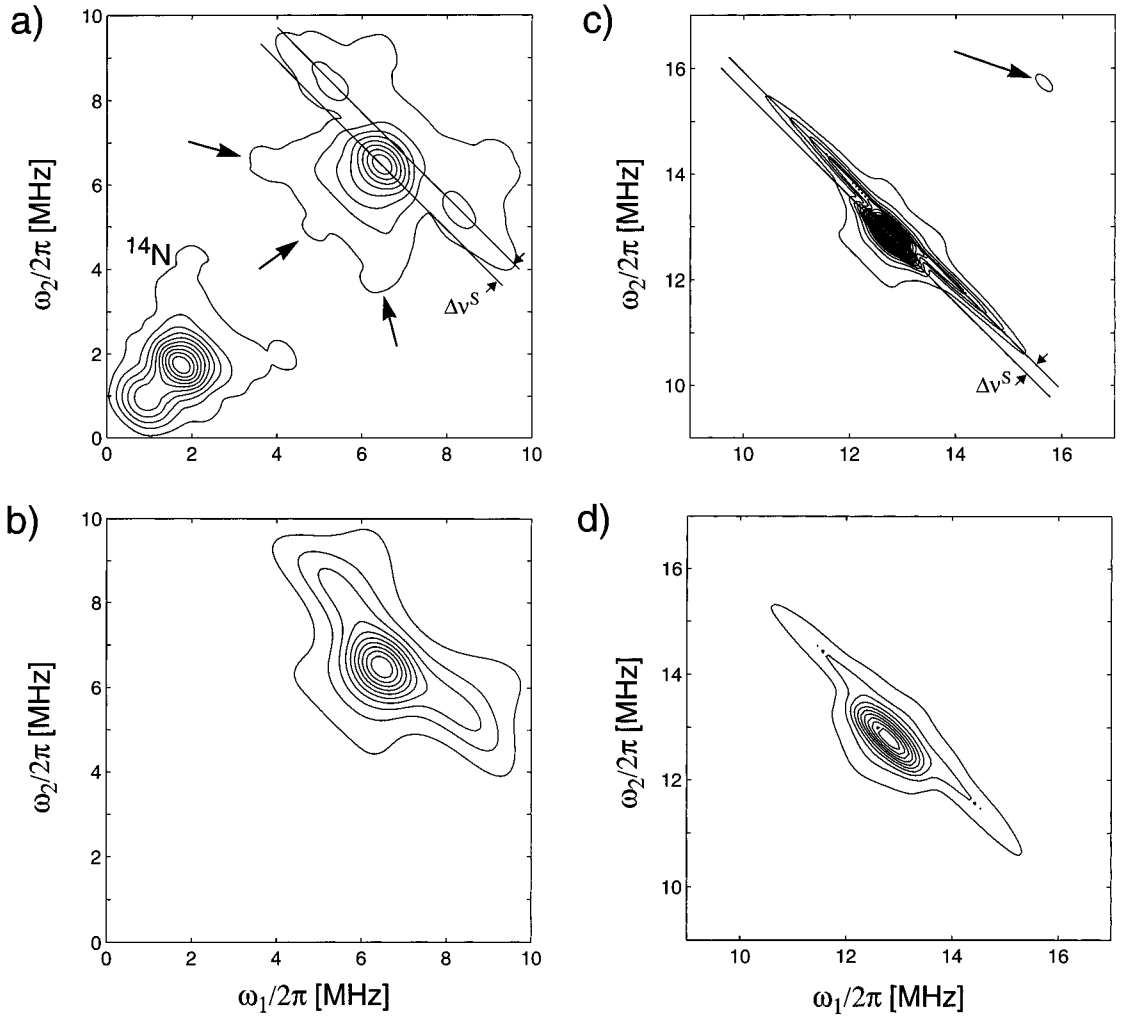

Figure 4. S-band and X-band HYSCORE spectra of CoTPP(py). (a) Spectrum taken at 3.7 GHz with $\mathbf{B_0} \parallel g_\parallel$ ($B_0 = 150$ mT). The weak peaks indicated by arrows are cross-peaks between the ^{14}N and ^{1}H frequencies and are not considered in the simulations. (b) Simulation of the proton HYSCORE spectrum in (a) using all hyperfine values of Table 2 and considering the number of nuclei contributing to each interaction (addition of the spectra weighted with number of nuclei). (c) Spectrum taken at 9.7 GHz with $\mathbf{B_0} \parallel g_\perp$ ($B_0 = 299$ mT, observer position III in inset in Figure 3). The peak indicated by an arrow is an instrumental artifact. (d) Simulation of the proton HYSCORE spectrum in (c) using all hyperfine values of Table 2 and considering the number of nuclei contributing to each interaction.

proton ENDOR lines partially overlap with the ^{14}N lines, the ENDOR spectra of CoTPP(py-d_5) and CoTPP([^{15}N]py) are also measured. From all these data, the hyperfine and nuclear quadrupole parameters can be evaluated through simulation (Table 3). The choice of the signs will be discussed later. For $\mathbf{B}_0 \parallel g_\perp$, a large number of orientations contribute to the ENDOR spectrum (hence the broad lines in Figure 5b), resulting in a relatively large error for the $Q_\perp^N$ value. A slight orthorhombicity of both **A** and **Q** cannot be excluded. The values for $A_\parallel^N$ derived from CW EPR (Table 1) and from the Davies-ENDOR experiments are the same within experimental error.

Interaction with the Nitrogen Nuclei of the Porphyrin Ligand. Since the unpaired electron is mainly localized in the d_{z^2}-orbital of the cobalt atom, the interaction with the four porphyrin nitrogens in the *xy*-plane is expected to be much smaller than the one with the nitrogen of the pyridine ligand. In the three-pulse ESEEM and HYSCORE spectra of CoTPP-(py), peaks at low frequencies are found that can be assigned to interactions with the porphyrin nitrogens. In the ENDOR spectra of Co[^{14}N]TPP(py) no signals in this frequency region can be found, but the corresponding Davies-ENDOR spectra of Co[^{15}N]TPP(py) show a peak in this region. Using the HYEND technique,[28] this signal could be assigned to a ^{15}N interaction (extrapolation of the ridge to zero hyperfine frequency resulted in the ν_{15_N} frequency). Corresponding ^{14}N ENDOR signals are not observed because $\nu_{15_N} > \nu_{14_N}$ (some lines are below the detection limit) and because the ^{14}N quadrupole interaction broadens the lines.

Figure 6a and b show the HYSCORE spectra of Co[^{15}N]-TPP(py) recorded with $\mathbf{B}_0 \parallel g_\perp$ (observer position III) and at

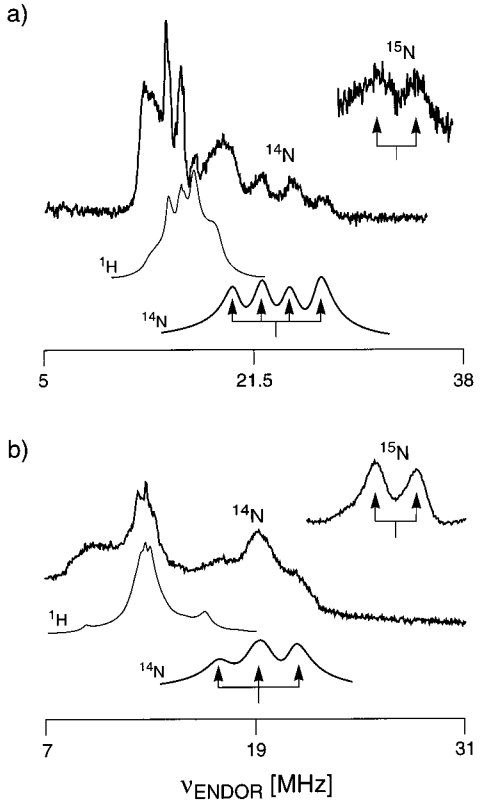

Figure 5. Davies-ENDOR spectrum of CoTPP([^{14}N]py) and CoTPP-([^{15}N]py): (a) High-field position $\mathbf{B_0} \parallel g_{\parallel}$, $m_I^{Co} = 7/2$ (observer position II in the inset of Figure 3), (b) $\mathbf{B_0} \parallel g_{\perp}$ (observer position III). The corresponding simulations of the proton and the ^{14}N(pyridine) ENDOR spectra are shown. The arrows indicate the positions of the nitrogen peaks.

the high-field end of the EPR spectrum ($\mathbf{B}_0 \parallel g_{\parallel}$, $m_I = {}^7/_2$, observer position II), respectively; Figures 6c and d show the corresponding simulated HYSCORE spectra. The spectra are typical for strongly coupled $I = {}^1/_2$ nuclei, since the ridges appear only in the (−,+)-quadrant. The separation of the ridges equals $2\nu_{15_N}$, revealing the type of nucleus responsible for the interaction. The simulation parameters are: $|A_{x''}| = 3.4$ MHz, $|A_{y''}| = 4.0$ MHz, $|A_{z''}| = 5.7$ MHz (errors: ±0.3 MHz) with $\beta = 95\ (\pm 5)^o$, where β is the angle between the $g_{\parallel}$ and $A_{z''}$-axis. $A_{x''}$ lies in the porphyrin plane perpendicular to $A_{z''}$. For each of the four porphyrin nitrogens the $A_{z''}$-axis is approximately along the Co−N_{porph} direction. This assignment will be elucidated in the discussion. It should be noted that the simulated spectrum 6c does not fully reproduce the shapes of the ridges found in the experiments (Figure 6a). The origin of this discrepancy could not be found. However, with these parameters good simulations of the Davies-ENDOR spectra are obtained (not shown). The absolute sign of the hyperfine principal values cannot be determined from the HYSCORE and the Davies-ENDOR spectra. To get the corresponding ^{14}N hyperfine couplings, the principal values have to be multiplied by $g_n(^{14}N)/g_n(^{15}N) = -0.7129$.

In Figure 6b, the cross peaks lie close to the frequency axes in the (−,+)-quadrant. This means that along the $g_{\parallel}$ direction (single-crystal like position), the cancelation condition[34] ($|A| \cong 2\nu_I$) is approximately fulfilled. With this orientation selection, the X-band HYSCORE spectrum of Co[^{14}N]TPP(py) shown in Figure 7a is therefore especially well suited to determine the nuclear quadrupole interaction parameters. In the (−,+) quadrant of this figure, three strong cross peaks with the double quantum frequency $\nu_{DQ}^{\beta} = 5.60$ MHz are observed (marked by arrows

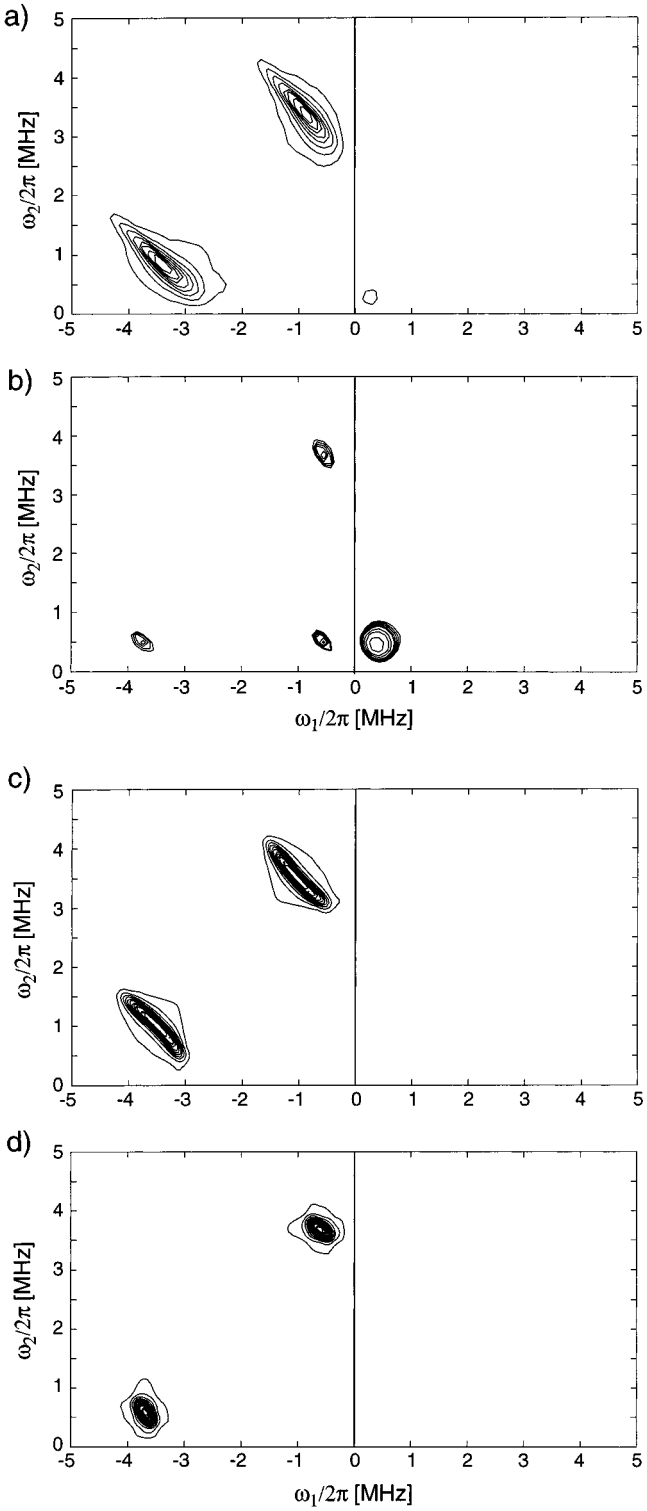

Figure 6. Experimental HYSCORE spectra of Co[^{15}N]TPP(py). (a) $\mathbf{B_0} \parallel g_{\perp}$ (observer position III in the inset in Figure 3), (b) $\mathbf{B_0} \parallel g_{\parallel}$, $m_I^{Co} = 7/2$ (observer position II), (c and d) corresponding simulations.

in Figure 7a), as is expected for cancelation. However, the sum of the two lower frequencies 0.60 and 1.75 MHz does not correspond to the third frequency 3.50 MHz. Although the four porphyrin nitrogen nuclei are expected to be geometrically equivalent with the same hyperfine coupling along $g_{\parallel}$, so that the 3.50 MHz peak can be considered as a combination peak of different nuclei, there still remains an ambiguity for the third nuclear quadrupole frequency which is not observed in this HYSCORE experiment (either 1.15 or 2.35 MHz). The

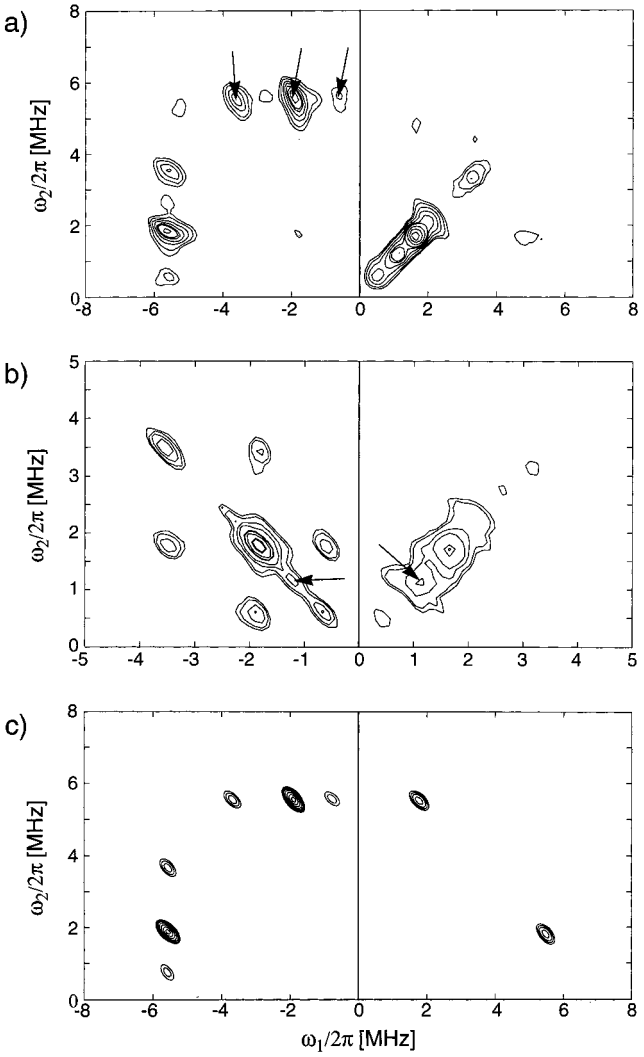

Figure 7. HYSCORE and DONUT−HYSCORE spectra of CoTPP-(py) at $\mathbf{B_0} \parallel g_{\parallel}$, $m_I^{Co} = {}^7/_2$ (observer position II in the inset of Figure 3). (a) HYSCORE spectrum (The arrows indicate the cross-peaks between frequencies of two m_S manifolds), (b) DONUT−HYSCORE spectrum (The arrows indicate the third NQR frequency), (c) simulation of the HYSCORE spectrum shown in (a).

weak cross peak found at (−2.50, 5.60) MHz is also not yet assigned.

To resolve this ambiguity, a DONUT−HYSCORE experiment[24,25] is done at the same observer position (Figure 7b). A cross peak is found at (−0.60, 1.75) MHz, indicating that 0.60 and 1.75 MHz are indeed two of the three expected nuclear quadrupole frequencies in the same m_S manifold. The frequency 1.75 MHz also correlates with its double frequency 3.50 MHz found in the HYSCORE spectrum. No further cross peaks are observed, but on the diagonal of the (−,+) quadrant, we find peaks at 0.60, 1.20, 1.75, 3.50, and 5.60 MHz (the last one is not shown). The peak at 1.20 MHz (marked with an arrow) suggests that this is the missing nuclear quadrupole frequency. The weak peak observed in the HYSCORE spectrum at (−2.50, 5.60) MHz may then be ascribed to a combination of different nitrogen nuclei ($2\nu_-$) (analogous to the 3.50 MHz frequency). Using the above assignment, we find for the pure NQR frequencies $\nu_0 \approx 0.60$ MHz, $\nu_- \approx 1.20$ MHz, and $\nu_+ \approx 1.75$ MHz. Using the formula given by Flanagan and Singel[33] (eq 10), starting values can be derived for e^2qQ/h and η. Simulations are found to be optimal for $e^2Qq/h = 1.8$ MHz and $\eta = 0.55$. These data are then used to simulate the experimental HY-

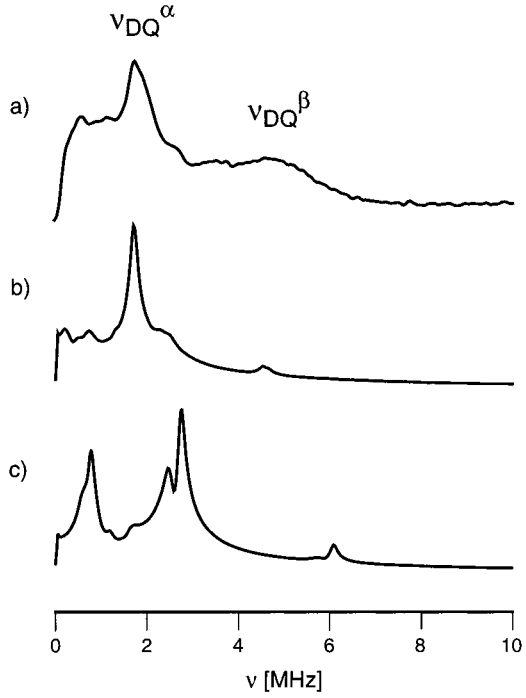

Figure 8. Three-pulse ESEEM spectrum of CoTPP(py) at $\mathbf{B_0} \parallel g_{\perp}$ (observer position III in inset in Figure 3). (a) Experiment (b) Simulation of (a) using the principal values of **A** and the data for e^2qQ and η given in Table 4 (1), with the largest (absolute) Q value along the $A_{z''}$-axis. The simulation shows the sum of the spectra at 10 different τ values ranging from 10 to 100 ns. (c) Simulation with the largest (absolute) Q value along the $A_{x''}$-axis.

SCORE spectra. The X-band simulation (high-field position, $\mathbf{B_0} \parallel g_{\parallel}$) is shown in Figure 7c. Since the simulation was done for ideal pulses, the diagonal peaks found in the (+,+) quadrant and caused by the incomplete coherence transfer governed by the π pulse between the two m_S states, are not reflected in the simulations. Using the above parameters, the DQ cross peak (−4.30, 2.80) MHz found in the (−,+) quadrant of the S-band HYSCORE spectrum at $g_{\parallel}$ (not shown), can also be explained.

From the HYSCORE spectra taken in the single crystal-like parallel direction, little information can be derived about the orientation of the **Q** tensor in the porphyrin plane. This information can be obtained from three-pulse ESEEM (Figure 8a) or HYSCORE spectra taken at $g_{\perp}$. Figure 8b and c show the simulations (using MAGRES[36]) of the spectrum, with the largest Q value (in absolute value) taken either along $A_{z''}$ or $A_{x''}$, respectively. Figure 8b obviously corresponds best to the experiment, implying that the axis of the largest hyperfine coupling is parallel to the axis of the largest quadrupole coupling (in absolute values). Both principal axes are directed along the $Co-N_{porph}$ bond as will be discussed later.

Discussion

g and A^{Co} Matrix. The ground state of Co(II)TPP(py) is found to be $(d_{xz})^2(d_{yz})^2(d_{xy})^2(d_{z^2})^1$.[41] Figure 9 shows the schematic molecular orbital diagram for CoTPP(L), where L is a Lewis base (e.g., pyridine). Wayland and Abd-Elmageed,[41] McGravey,[42] and Baumgarten[12] calculated the electron spin density on the cobalt atom for a series of Co(II) complexes with d_{z^2} ground state. The spin density lies in the range $0.70 \leq \rho_{3d} \leq 0.97$ for the 3d orbitals and in the range $0.02 \leq \rho_{4s} \leq 0.09$ for the 4s orbital. Using the simple expressions given by Wayland and Abd-Elmageed,[41] based on Maki et al.,[43] values of $\rho_{3d} = 0.85$ and $\rho_{4s} = 0.04$ can be calculated from our experimental

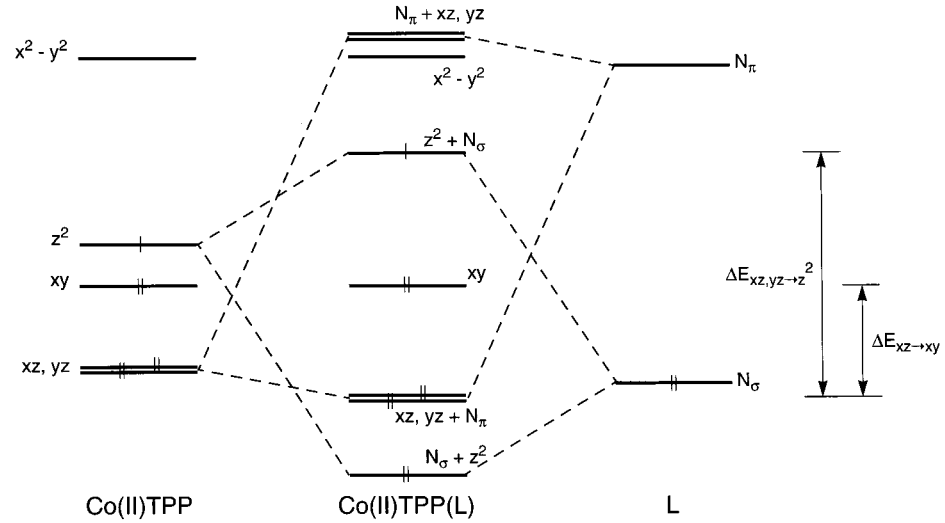

Figure 9. Schematic molecular orbital diagram for Co(II)TPP(L); L represents a Lewis base.

$\mathbf{A}^{Co}$ and **g** matrixes of CoTPP(py). The corresponding energy difference $\Delta E_{xz,yz\rightarrow z^2}$ is estimated to be about 8200 cm^{-1}. The formulas used by Wayland and Abd-Elmageed[41] were optimized by McGravey,[42] Attanasio et al.[44] and Baumgarten.[12] For CoOEP(py), which is very similar to CoTPP(py), Baumgarten[12] found a total spin density at the cobalt of $\rho(Co) = 0.95$ ($\rho_{3d} = 0.90$ and $\rho_{4s} = 0.05$) and values of 8380 and 3620 cm^{-1} for the energy differences $\Delta E_{xz,yz\rightarrow z^2}$ and $\Delta E_{xz\rightarrow xy}$, respectively. The corresponding values for CoOEP in tetrahydorfuran(THF)/toluene are 4840 and 3240 cm^{-1}, respectively.[12] In the latter compound, THF acts as a weak axial ligand. The large increase of $\Delta E_{xz,yz\rightarrow z^2}$ upon addition of the pyridine base indicates the destabilization of the d_{z^2} orbital relative to the d_{xz} and d_{yz} orbitals. The fact that $\Delta E_{xz\rightarrow xy}$ increases much less than $\Delta E_{xz,yz\rightarrow z^2}$, shows that the σ donor contribution plays a dominant role in the addition of the pyridine base (see Figure 9).

Interaction with the Surrounding Protons. In Table 2, the principal values of the different proton hyperfine couplings, the orientations of the principal axes, the distances r between the different protons and the Co^{2+} ion and the values of a_{iso} are collected. Taking $\rho(Co) = 0.90$, gives only a small change in the distance r (<0.01 nm). The largest coupling (1) is due to the interaction with the ortho-H of pyridine (position 2′ and 6′, Figure 1). Combination of the simulation parameters of interaction (2) and the X-ray data of pyridine[45] (C−H bond length was taken 0.1 nm), allows the assignment of this coupling to the meta-H of the pyridine in positions 3′ and 5′. The smallest observable coupling (3) is due to the eight porphyrin ring protons in positions 2, 3, 7, 8, 12, 13, 17, and 18. The couplings of the phenyl protons and the pyridine proton 4′ are very weak and contribute to the signal at the proton Zeeman frequency.

Note that Baumgarten[12] in his CW ENDOR study of CoOEP-(py) could not observe isotropic proton splittings larger than 0.79 MHz. This is very surprising in view of the close similarity of the two systems. It is known however that very broad peaks are difficult to observe with CW ENDOR, in particular when the spectra are recorded as first derivatives. In CoTPP(py), Däges et al.[14] observed weak peaks with a splitting of about 8 MHz which were assigned to an interaction with the closest pyridine protons, but the corresponding hyperfine interactions were not determined.

Interaction with the Nitrogen Nucleus of the axial Pyridine Ligand. From the position of the pyridine protons 2′ and 6′ and the X-ray data of the pyridine molecule[45] (C−H bond length taken 0.1 nm), the distance $Co-N_{py}$ can be estimated as 0.23 nm. This can be compared with the value of 0.2161 nm found from an X-ray study of CoTPP(3,5-dimethylpyridine).[46] Considering the **g** anisotropy, the calculated distance leads to a nontraceless point−dipolar contribution to the ^{14}N hyperfine matrix of (−0.5, −0.5, 0.9) MHz (eqs 8 and 9). The sign of the observed pyridine nitrogen interaction is taken to be positive in accordance with previous studies.[14] The hyperfine matrix can be split into an isotropic part a_{iso} and two anisotropic parts

$$\begin{bmatrix}38.2\ \text{MHz}\\38.2\ \text{MHz}\\47.4\ \text{MHz}\end{bmatrix} = 41.3\ \text{MHz} + \begin{bmatrix}-0.5\ \text{MHz}\\-0.5\ \text{MHz}\\0.9\ \text{MHz}\end{bmatrix} + \begin{bmatrix}-2.6\ \text{MHz}\\-2.6\ \text{MHz}\\5.2\ \text{MHz}\end{bmatrix}$$

From a_{iso}, a spin density on the nitrogen nucleus $\rho^N = 0.027$ ($\rho^N = a_{iso}/a_0$ with $a_0 = 1538.22$ MHz[47]) can be calculated. The anisotropic part is the sum of the point-dipole part and the contribution (−2.6, −2.6, 5.2) MHz. The latter axial part reflects that the overlap and mixing of the pyridine σ donor orbital with the cobalt d_{z^2} directly places spin density in the ligand σ system (see Figure 9). The values of a_{iso} for the pyridine proton hyperfine couplings (Table 2) indicate that the unpaired electron is also delocalized to some extend throughout the pyridine ring.

For the pyridine ^{14}N nuclear quadrupole interaction given in Table 3, we evaluate $|e^2qQ/h| = 3.4$ MHz and $0 \le \eta \le 0.3$. Hsieh et al.[48] found from nuclear quadrupole resonance experiments the values $|e^2qQ/h| = 4.584$ MHz and $\eta = 0.396$ for the free pyridine molecule. These authors also observed that, upon coordination of pyridine with a Lewis acid (here CoTPP), the electric field gradient at the nitrogen nucleus decreases, which is confirmed by our measurement. Furthermore, they found a linear relation between $|h/(e^2qQ)|$ and η. Using their simplified equation, the value of $|e^2qQ/h| = 3.4$ MHz results in $\eta = 0.28$, which is in good agreement with our measurements. Brown and Hoffman[49] found that the largest nuclear quadrupole coupling is negative when it is oriented along the metal−N bond. This justifies our choice of the signs for $Q_{||}^N$.

Table 3 also shows the hyperfine and nuclear quadrupole values of the pyridine nitrogen interaction in CoTPP(py) reported by Däges et al..[14] The authors observed in the CW ENDOR spectrum at least six nitrogen lines along $g_{||}$. They interpreted the two additional lines as a doublet with zero quadrupole interaction, although a second species contributing with a different coupling scheme was not excluded. We assume a six-line pattern has been recorded because the observer field was not properly chosen at the high-field end of the EPR

TABLE 4: ^{14}N Hyperfine and Nuclear Quadrupole Parameters for Different Porphyrin Systems and for *trans*-Bis(dimethylglyoximato)bis(pyridine)cobalt(II)(Co(II)(dmg)$_2$(py)$_2$)[a]

	$A_{x''}$ (MHz)	$A_{y''}$ (MHz)	$A_{z''}$ (MHz)	ρ^N	$\lvert e^2qQ/h\rvert$ (MHz)	η	ref
(**1**) CoTPP(py)	2.43	2.85	4.07	0.002	1.8	0.55	this work
(**2**) CuTPP	42.778	44.065	54.213	0.031	1.85	0.34	49
(**3**) AgTPP	61.33	62.918	78.87	0.044	1.83	0.51	49
(**4**) cytochrome-d	6.5	7.0	8.2	0.024	2.60	0.49	51
	7.1	7.1	9.3	0.026	2.66	0.51	
(**5**) hemin	6.1	6.8	7.7	0.023	2.24	0.51	51
	6.7	6.7	8.6	0.024	2.30	0.51	
(**6**) metmyoglobin	6.7	6.9	8.3	0.024	2.44	0.51	51
	7.2	6.9	9.2	0.025	2.26	0.51	
(**7**) aquometmyoglobin	6.89	7.11	9.86	0.026	2.08	0.48	52
(**8**) Fe(III)TPP(py)(OR$^-$)	5.1	4.9	4.6	0.003	2.2	0.2	53
(**9**) myoglobin hydroxide	5.1	5.3	4.9	0.003	2.2	0.1	53
(**10**) VOTPP	2.91	8.01	9.5	0.004	0.86	0.21	54
(**11**) Co(II)(dmg)$_2$(py)$_2$	1.84	1.86	2.61	0.001	3.4	0.7	55

[a] In all cases the y''-axis is approximately perpendicular to the equatorial plane. For each porphyrin nitrogen the z'' axis is along the N_{porph}−metal bond. For the complexes **2**−**7** and **10**, the largest Q value lies in the porphyrin plane, perpendicular to this N_{porph}−metal bond. For compounds **1** and **11**, this Q value lies along the N−metal bond, and in complexes **8** and **9** the $Q_{z''}$ axis makes an angle of 48° with the g_z axis ($Q_{x''}||A_{x''}$).

spectrum, so that a powder-like rather than a single crystal-like spectrum was observed. Measurements at the high-field position ($m_I^{Co} = {}^7/_2$) clearly reveal four lines, as is shown in Figure 5a. The large discrepancies between the parameters of ref 14 and our data in the $g_{||}$ direction can be explained in the same way.

Greiner and Baumgarten[13] reported for the pyridine nitrogens of the CoOEP(py) complex a slightly rhombic hyperfine interaction (Table 3). The rhombicity is, however, within the experimental error. More puzzling are the values they obtained for the **Q** tensor. The largest coupling (in absolute values) does not point along the N−Co axis. These results are in contradiction with ours and those reported by Däges et al.[14] A possible explanation might be that a signal of the largest proton coupling was falsely ascribed to the nitrogen interaction.

Interaction with the Nitrogen Nuclei of the Porphyrin Ligand. The hyperfine couplings of the porphyrin nitrogens (Table 4) are much smaller than the hyperfine couplings of the pyridine nitrogen. The ^{14}N hyperfine interaction can again be split into an isotropic part and an anisotropic part

$$\begin{bmatrix}2.43\ \text{MHz}\\ 2.85\ \text{MHz}\\ 4.07\ \text{MHz}\end{bmatrix} = 3.12\ \text{MHz} + \begin{bmatrix}-0.69\ \text{MHz}\\ -0.27\ \text{MHz}\\ 0.95\ \text{MHz}\end{bmatrix}$$

The a_{iso} value of 3.12 (±0.2) MHz corresponds to a spin density on the nitrogen nucleus ρ^N of 0.0020 (±0.0002). Our previous assignment of the $A_{z''}$ axis to a Co−N_{porph} direction can be justified by the fact that the anisotropic part is mainly governed by the N−Co point-dipolar interaction. Considering the experimental errors of the hyperfine interactions and using eqs 8 and 9, the Co−N distance obtained from the anisotropic part is estimated to 0.23 ± 0.03 nm. The X-ray analysis of CoTPP(3,5-dimethylpyridine)[46] shows that the Co−N_{porph} distance in this complex is 0.20 nm, which is slightly lower than our value. Due to the experimental error of about 200 kHz, it is difficult to determine whether the orthorhombicity of the anisotropic part is governed by spin density in the nitrogen p_π orbital or if it can be fully ascribed to the **g** anisotropy. If the signs of the hyperfine interaction are taken negative, the observed anisotropic part cannot be explained satisfactorily. The fact that the angle β slightly deviates from 90° seems to be an indication that the cobalt ion is above the porphyrin ring (in the direction of the pyridine ligand). X-ray data of several pentacoordinated cobalt porphyrin complexes indeed mention out-of-plane displacements of about 0.018 nm.[46,50] The displacement, calculated from β and the Co−N_{porph} distance r, is found to be 0.019 (± 0.019) nm. However, because of the large error, the result cannot be considered as a proof of an out-of-plane displacement, but at least it shows that such a displacement of the cobalt ion is not in disagreement with our measurements.

The hyperfine and nuclear quadrupole parameters of the porphyrin nitrogens of different metalloporphyrins are given in Table 4. The values of the spin density at the nitrogen nucleus ρ^N calculated as a_{iso}/a_0 with $a_0 = 1538.22$ MHz[47] give a measure for the transfer of electron spin density from the metal ion on the porphyrin nitrogens. Note that for the compounds **4**−**7**, the fact that an $S = {}^5/_2$ system is present is taken into account for the calculation of ρ^N.

In CuTPP (**2**) and AgTPP (**3**), the unpaired electron resides mainly in the metal $d_{x^2-y^2}$ orbital, resulting in a strong overlap with the sp^2 hybrid orbitals of the porphyrin nitrogens. Brown and Hoffman[49] showed that the unpaired electron is further delocalized in the porphyrin ring ($a_{iso} = 1.3$ and 2.1 MHz for the porphyrin protons 2, 3, 7, 8, 12, 13, 17, and 18 in CuTPP and AgTPP, respectively.). Both the observed a_{iso} value of 0.1 MHz for the corresponding protons and the ρ^N value for the porphyrin nitrogens of CoTPP(py) reflect that the spin density in the ring is a factor 15−20 smaller than that in CuTPP and AgTPP.

For the high-spin ($S = {}^5/_2$) iron porphyrin systems **4**−**7**, a large interaction with the nitrogens of the porphyrin ring is expected, which is reflected in the ρ^N values (approximately a factor 10 larger as the corresponding value for CoTPP(py)). In VOTPP (**10**) the unpaired electron is in a molecular orbital with dominant metal−ion d_{xy} orbital contribution. The interaction with the porphyrin nitrogens is smaller than in the case of AgTPP and CuTPP, because the lobes of the d_{xy} bisect the N−V−N bond angles, so that there is minimal overlap with the ligand orbitals. For CoTPP(py) (unpaired electron in the d_{z^2} orbital) and the compounds **8** and **9** (unpaired electron in d_{yz}), again a small spin density is expected on the porphyrin nitrogens. This is also in agreement with the studies of Wirt et al.[55] on *trans*-bis(dimethylglyoximato)bis(pyridine)cobalt(II) (**11**), (Co(II)(dmg)$_2$(py)$_2$), where a value $a_{iso} = 2.1$ MHz for the isotropic hyperfine coupling with the dmg nitrogens was derived from three-pulse ESEEM. The unpaired electron is here in the d_{z^2} orbital.

There is a surprising similarity between the nuclear quadrupole parameters $\lvert e^2qQ/h\rvert$ and η found for the porphyrin nitrogens in CoTPP(py) and the compounds **2**−**7**. This similarity must however be accidental, since in CoTPP(py) the direction of the

largest coupling (in absolute value) is along the $Co-N_{porph}$ bond and for the complexes **2**−**7** it is in the porphyrin plane perpendicular to the metal−N_{porph} bond. The orientation of the nuclear quadrupole tensor in CoTPP(py) corresponds to the one found in $Co(II)(dmg)_2(py)_2$ ($\beta = 95°$).[55] This suggests that for the Co(II) complexes discussed here, the direction of the largest nuclear quadrupole coupling is determined by the orientation of the lone pair nitrogen donor orbitals, in contrast to the compounds **2**−**7**. Brown and Hoffman[49] found from model calculations that the largest nuclear quadrupole coupling is negative, when it is oriented along the metal−N bond, as is found for example for free pyridine and imidazole, hence, the absolute sign we propose for the nuclear quadrupole coupling in CoTPP(py).

Conclusion

The cobaltous tetraphenylporphyrin(pyridine) complex is studied in great detail using different one- and two-dimensional pulse EPR and ENDOR methods. The hyperfine interactions with the ortho and meta protons of pyridine and with the protons of the porphyrin ligand can be evaluated using pulse ENDOR and HYSCORE. For the first time, the importance of S-band HYSCORE to investigate anisotropic proton couplings is shown. Davies-ENDOR is found to be very useful to determine the hyperfine and nuclear quadrupole interaction with the nitrogen nucleus of the pyridine ligand. Incorrect interpretations given in the literature (because of a lack of sufficient information) could be revealed. In the lower frequency region of the three-pulse ESEEM and HYSCORE spectra signals due to the interactions with the porphyrin nitrogens are found. The use of the DONUT−HYSCORE technique facilitates the interpretation of these HYSCORE spectra. The corresponding set of small hyperfine and nuclear quadrupole couplings is determined with the help of extensive spectrum simulations. From the hyperfine data, internuclear distances are calculated and the distribution of the spin density in the complex was determined. The parameters are compared with the ones of other metalloporphyrin systems. This study demonstrates that pulse EPR and ENDOR techniques at X- and S-band provide a very powerful tool to investigate the electronic and geometric structure of metalloporphyrin. It also gives an insight in which methods can be used to study interactions with different types of nuclei and different values of the couplings.

Acknowledgment. This research has been supported by the Swiss National Science Foundation. Dr. Gunnar Jeschke is gratefully acknowledged for helpful discussions and suggestions.

References and Notes

(1) Walker, F. A. *J. Am. Chem. Soc.* **1970**, *92*, 4235.
(2) Smith, T. D.; Pilbrow, J. R. *Coord. Chem. Rev.* **1981**, 39, 295.
(3) Jones, R. D.; Summerville, D. A.; Basolo, F. *Chem. Rev.* **1979**, *79*, 139.
(4) Hoffman, B. M.; Petering, D. H. *Proc. Natl. Acad. Sci. U.S.A.* **1970**, 67, 637.
(5) Ikeda-Saito, M.; Brunori, M.; Yonetani, T. *Biochim. Biophys. Acta* **1978**, 533, 173 and references therein.
(6) Dickinson, L. C.; Chien, J. C. W. *Proc. Natl. Acad. Sci U.S.A.* **1980**, 77, 1235.
(7) (a) Hori, H.; Ikeda-Saito, M.; Yonetani, T. *Nature* **1980** 288, 501. (b) Hori, H.; Ikeda-Saito, M.; Yonetani, T. *J. Biol. Chem.* **1982**, 257, 3636.
(8) Walker, F. A., *J. Am. Chem. Soc.* **1973**, *95*, 1154.
(9) Walker, F. A. *J. Magn. Reson.* **1974,** 15, 201.
(10) Iwaizumi, M.; Ohba, Y.; Iida, H.; Hirayama, M. *Inorg. Chim. Acta* **1984**, 82, 47.
(11) Bowen, J. H.; Shokhirev, N. V.; Raitsimring, A. M.; Buttlaire, D. H.; Walker, F. A. *J. Phys. Chem. B* **1997**, 101, 8683.
(12) Baumgarten, M. EPR und ENDOR Untersuchungen an Übergangsmetallkomplexen mit organischen Chelatliganden−Modellsysteme für katalytische und biologische Prozesse, Ph.D. Thesis, Free University of Berlin, 1988.
(13) Greiner, P.; Baumgarten, M. *J. Magn. Reson.* **1989,** 83, 630.
(14) Däges, G. P.; Hütterman, J. *J. Phys. Chem.* **1992**, 96, 4787.
(15) Schweiger, A., *Angew. Chem., Int. Ed. Engl.* **1991**, 30, 265.
(16) Gemperle, C.; Schweiger, A. *Chem. Rev.* **1991**, *91*, 1481.
(17) Magliozzo, R.; McCracken, J.; Peisach, J. *Biochemistry* **1987**, *26*, 7923.
(18) Lee, H. C.; Scheuring, E.; Peisach, J.; Chance, M. R. *J. Am. Chem. Soc.* **1997**, *119*, 12201.
(19) Willer, M. *Low-frequency pulse electron spin resonance spectroscopy*, Ph.D. Thesis, ETHZ 12201, 1997.
(20) Dikanov, S. A.; Tsvetkov, Y. D. *Electron Spin−Echo Modulation Spectroscory*; CRC: Boca Raton, 1992.
(21) Höfer, P.; Grupp, A.; Nebenführ, H.; Mehring, M. *Chem. Phys. Lett*. **1986**, 132, 279.
(22) Hubrich, M.; Jeschke, G.; Schweiger, A. *J. Chem. Phys*. **1996**, 104, 2172.
(23) Ponti, A.; Schweiger, A. *J. Chem. Phys.* **1995**, 102, 5207.
(24) Hoffmann, E.; Hubrich, M.; Schweiger, A. *J. Magn. Reson.* **1995**, A117, 16.
(25) Goldfarb, D.; Kofman, V.; Libman, J.; Shanzer, A.; Rakhmatullin, R.; Van Doorslaer, S.; Schweiger, A. *J. Am. Chem. Soc.* **1998**, 120, 7020.
(26) Mims, W. B. *Proc. R. Soc.* **1965**, 283, 452.
(27) Davies, E. R. *Phys. Lett.* **1974**, A 47, 1.
(28) Jeschke, G.; Schweiger, A. *Chem. Phys. Lett.* **1995**, 246, 431.
(29) Rist, G.; Hyde, J. *J. Chem. Phys.* **1970**, 52, 4633.
(30) Pöppl, A.; Kevan, L. *J. Phys. Chem.* **1996**, 100, 3387.
(31) Anderson, M. W.; Kevan, L. *J. Phys. Chem.* **1986**, 90, 6542.
(32) Hurst, G. C.; Henderson, T. A.; Kreilick, R. W. *J. Am. Chem. Soc.* **1985**, *107*, 7294.
(33) Hoffman, B. M.; Martinsen, J.; Venters, R. A. *J. Magn. Reson*. **1984**, 59, 110.
(34) Flanagan, H. L.; Singel, D. J. *J. Chem. Phys*. **1987**, 87, 5606.
(35) Dikanov, S. A.; Xun, L.; Karpiel, A. B.; Tyryshkin, A. M.; Bowman, M. K. *J. Am. Chem. Soc.* **1996**, *118*, 8408.
(36) Keijzers, C. P., Reijerse, E. J., Stam, P., Dumont, M. F.; Gribnau, M. C. M *J. Chem. Soc., Faraday Trans. 1* **1987,** 83, 3493.
(37) Dikanov, S. A.; Bowman, M. K. *J. Magn. Reson.* **1995**, *A116*, 125.
(38) Szosenfogel, R.; Goldfarb, D. *Mol. Phys.* **1998**, *95*, 1295.
(39) Smith, S. A.; Levante, T. O.; Meier, B. H.; Ernst, R. R. *J. Magn. Reson.* **1994**, A106, 75.
(40) Thomann, H.; Bernardo, M. *Methods Enzymol.* **1993**, 227, 118.
(41) Wayland, B. B.; Abd-Elmageed, M. E. *J. Am. Chem. Soc.* **1974**, *96*, 4809
(42) McGarvey, B. R. *Can. J. Chem*. **1975**, 53, 2498.
(43) Maki, A. H.; Edelstein, N.; Davison, A.; Holm, R. H. *J. Am. Chem. Soc.* **1964**, 86, 4580.
(44) Attanasio, D.; Dessy, G.; Fares, V.; Pennesi, G. *Mol. Phys.* **1980**, 40, 269.
(45) Mata, F.; Quintana, M. J.; Sörensen, G. O. *J. Mol. Struct.* **1977**, 42, 1.
(46) Scheidt, W. R.; Ramanuja, J. A. *Inorg. Chem.* **1975**, *11*, 2643.
(47) Koh, A. K.; Miller, D. J. *At. Data Nucl. Data Tables* **1985**, 33, 235.
(48) Hsieh, Y.-N.; Rubenacker, G. V.; Cheng, C. P.; Brown, T. L. *J. Am. Chem. Soc.* **1977**, *99*, 1384.
(49) Brown, T. G.; Hoffman, B. M. *Mol. Phys.* **1980**, 39, 1073.
(50) Scheidt, W. R. In *The Porphyrins*, Dolphin, D., Ed.; Academic Press: New York, 1978; Vol. III, pp 463−511.
(51) Jiang, F. S.; Zuberi, T. M.; Cornelius, J. B.; Clarkson, R. B.; Gennis, R. B.; Belford, R. L. *J. Am. Chem. Soc*., **1993**, 115, 10293.
(52) Scholes, C. P.; Lapidot, A.; Mascarenhas, R.; Inubushi, T.; Isaacson, R. A.; Feher, G. *J. Am. Chem, Soc*, **1982**, 104, 2724.
(53) Magliozzo, R. S.; Peisach, J. *Biochemistry*, **1992**, 31, 189.
(54) Mulks, C. F.; van Willigen, H. *J. Phys. Chem.* **1981**, 85, 1220.
(55) Wirt, M. D.; Bender, C. J.; Peisach, J. *Inorg. Chem.* **1995**, 34, 1663.